X-Ray Nanointerferometer Based on Si Refractive Bilenses

A. Snigirev,[1] I. Snigireva,[1] V. Kohn,[2] V. Yunkin,[3] S. Kuznetsov,[3] M. B. Grigoriev,[3] T. Roth,[1] G. Vaughan,[1] and C. Detlefs[1]

[1]*ESRF, B.P. 220, 38043 Grenoble, France*

[2]*Russian Research Center "Kurchatov Institute," 123182, Moscow, Russia*

[3]*IMT RAS, 142432 Chernogolovka, Moscow region, Russia*

(Received 28 April 2009; published 3 August 2009)

We report a novel type of x-ray interferometer employing a bilens system consisting of two parallel compound refractive lenses, each of which creates a diffraction limited beam under coherent illumination. By closely overlapping such coherent beams, an interference field with a fringe spacing ranging from tens of nanometers to tens of micrometers is produced. In an experiment performed with 12 keV x rays, submicron fringes were observed by scanning and moiré imaging of the test grid. The far field interference pattern was used to characterize the x-ray coherence. Our technique opens up new opportunities for studying natural and man-made nanoscale materials.

DOI: 10.1103/PhysRevLett.103.064801 PACS numbers: 41.50.+h, 07.85.Qe, 61.05.cp

Conventional hard x-ray radiography underwent tremendous progress due to the passage from absorption contrast to a phase shifting mechanism of image formation. With the appearance of new synchrotron radiation sources providing brilliant and highly coherent x-ray beams, inline phase contrast imaging techniques have been proposed [1–4]. Free space propagation methods remain the most widely used techniques for radiography in transmission geometry; they find a wide spectrum of applications in material and life sciences and chemistry, as well as in biological and medical studies. Taking advantage of the laserlike properties of synchrotron x-ray beams allows one to develop inline or paraxial schemes of x-ray interferometry. A striking example of the effectiveness of x-ray interferometry is the grating interferometer [5–7] in which a spatially modulated x-ray beam is used to provide complementary and otherwise inaccessible information about the specimen at the micrometer scale. However, the resolution of this technique is determined by modulation pitch size which is limited by the grating pitch and therefore restricted to a micrometer scale.

The availability of a spatially periodic illuminating field or standing waves with a length scale below a micrometer would allow the investigation of the new generation of man-made and natural nanoscale materials, such as self-organized biological systems, photonic crystals, nanoelectronics materials, and crystals with large lattice spacing. One way of producing such periodically modulated beams is the classical Young's double slit experiment where interference of two coherent beams created by two narrow slits occurs. Although this is a quite challenging technological task, this interference has been demonstrated [8–10]. However, its applicability is limited due to significant loss of intensity and low resolution.

Refractive optics for high energy x rays have been successfully demonstrated and are now mature and widely implemented [11–14]. In this Letter, we propose an x-ray bilens interferometer similar to the model of a Billet split lens [15] in classical optics. The schematic diagram of our x-ray bilens interferometer is shown in Fig. 1. It consists of two identical, parallel planar compound refractive lenses separated transversally by a distance d. Each lens focuses the beam at a distance $z_f = F/(1 - F/z_0)$, where $F = R/2N\delta$ is the lens focal length, z_0 is the source-to-bilens distance, R is the radius of curvature of one parabolic surface, N is the number of elements in the lens, and δ is the decrement of refraction index $n = 1 - \delta + i\beta$.

Similar to the Young double slit scheme, the split distance d of the bilens should be smaller than the spatial

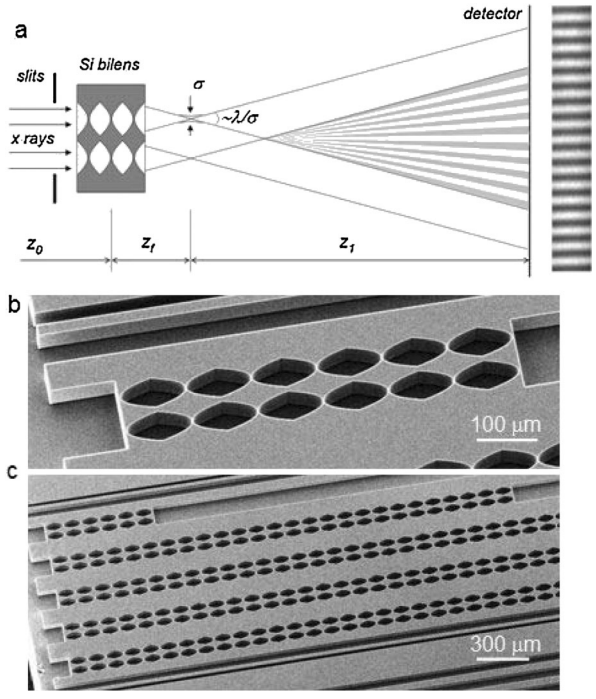

FIG. 1. (a) Schematic view of the x-ray bilens interferometer. (b) Scanning electron microscope micrograph of a single silicon bilens consisting of 6 individual parabolic lenses. (c) General view with five bilens systems fabricated on the same substrate.

coherence length of the incoming beam defined as $l_{\mathrm{coh}} = \lambda z_0/S$, where S is the effective source size (FWHM). As a consequence, each lens is illuminated coherently, and therefore it generates a coherent, diffraction limited focal spot of size $\sigma = \lambda z_f/A_{\mathrm{eff}}$. Here $A_{\mathrm{eff}} = 0.47(\lambda R/N\beta)^{1/2}$ is the absorption limited effective aperture of the lens, where β is the index of absorption and λ is the wavelength [11]. At a distance $z_1 > z_f d/A_{\mathrm{eff}}$, the cones diverging from these secondary sources overlap, and in this region of superposition interference occurs. The fringe spacing or peak-to-peak width of fringes is given by $\Lambda = \lambda z_1/d$. It should be noted that this interference pattern is laterally nonlocalized; i.e., it exists everywhere within the region of overlap. It has a variable period ranging from tens of nanometers to tens of micrometers, depending on the distance z_1.

The planar parabolic bilenses were manufactured using a process involving electron beam lithography and deep etching into silicon [14]. The length and aperture of each single, double concave individual lens are 102 and 50 μm, respectively. Structures are 70 μm deep. The radius of the parabola apex is $R = 6.25$ μm, and the minimum thickness between the parabola apexes is 2 μm. The split distance between lenses is $d = 60$ μm. A scanning electron microscope image of the bilens interferometer is shown in Fig. 1(b). In order to obtain a reasonably short focal distances at higher energies, five bilens interferometers were manufactured on the same Si chip. They differ in the number of individual lenses covering a range of x-ray energies from 10 to 50 keV [Fig. 1(c)].

The experimental tests of the bilenses were carried out at the ESRF beam line ID06. A liquid nitrogen cooled Si-111 double crystal, fixed exit monochromator was used to adjust an x-ray energy in the range 10–20 keV. The Si bilens system was mounted at a distance $z_0 = 54.16$ m from the source. Interference patterns were recorded by means of the high resolution x-ray CCD camera with a spatial resolution about 1.3 μm (0.645 μm pixel size).

To record the interference pattern in the far field, the CCD camera was placed at the distance $z_d = z_f + z_1 = 3.94$ m from the bilens. The typical exposure time was 5–10 seconds during a 16 bunch mode with 90 mA max stored current. The observed interference pattern and intensity variation of the fringe pattern are shown in Fig. 2. The measured fringe spacing was $\Lambda = 6.25$ μm, in very good agreement with calculations.

The quality of the fringes produced by a bilens system can be described quantitatively using the visibility V:

$$V = \frac{I_{\max} - I_{\min}}{I_{\max} + I_{\min}} = \exp\left[-\frac{\pi^2}{4\ln 2}\left(\frac{S(z_f + z_1)}{\Lambda z_0}\right)^2\right]. \quad (1)$$

Here $I_{\max}$ and $I_{\min}$ are the irradiances corresponding to the maximum and adjacent minimum in the fringe system, respectively. The formula is obtained as a convolution of sinusoidal intensity profile with the period Λ and a source size projection intensity distribution of the Gauss shape. The numerical coefficient is equal to 3.56. As for the Young double slit, the visibility is a function of the source size and can be used as a measure of the degree of a spatial coherence or of an effective source size. Using Eq. (1), we obtain the following expression for the effective source size:

$$S = \frac{\Lambda z_0}{(z_f + z_1)}\left(-\frac{\ln V}{3.56}\right)^{1/2}. \quad (2)$$

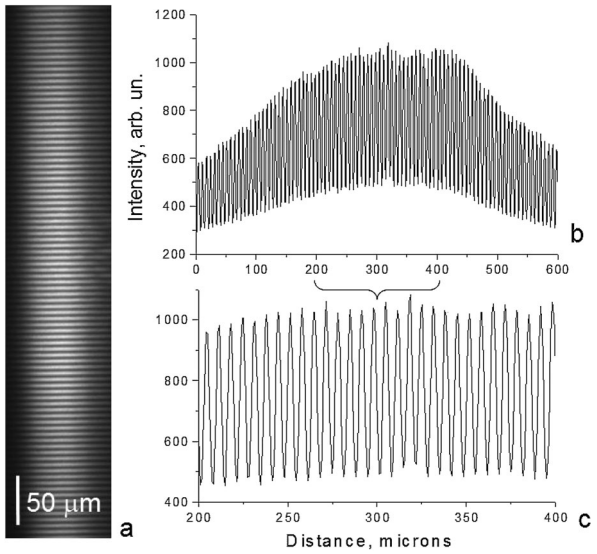

FIG. 2. An interference pattern (a) generated by a second bilens system, recorded at a 1 Å wavelength. The intensity variation (b) obtained for the line though the center of the fringe pattern and (c) insert showing a visibility of approximately 38%.

The measured value of the visibility was about 38% [Fig. 2(c)]. From this it follows that the effective source size in a vertical direction was 45 ± 5 μm (FWHM). This value coincides with data found by interferometry techniques (see [16] for details). It should be noted that for all 5 bilenses the recorded interference patterns showed the same visibility, around $38 \pm 2\%$, as expected from Eq. (1), as $z_f \ll z_1$. Considering that the lens effective aperture A_{eff} changes by a factor of 5 and that the number of concave surfaces changes by a factor of 27 from set 1 to set 5, we conclude that the lens quality is excellent. This was verified by measuring the focusing properties of individual lenses from bilens set 2 by the knife-edge scanning technique. A focus of 130 nm (FWHM) was measured, showing the theoretical diffraction limit for $E = 12$ keV.

The bilens interferometer presented here exhibits major advantages over other interferometer schemes taken from classical optical such as Young double slits, Fresnel double mirrors, or biprisms. Manufacturing of microslits, mirrors, and prisms for hard x rays is a challenging technological task considering the requirements to the surface and shape (edges) quality. In contrast, for silicon planar lenses, well-developed microelectronics technology is used providing superior lens quality [14]. Using a bilens interferometer, the coherence length can be extracted from the measured data without any prior assumption of its shape. Also, unlike

slits [8–10], mirrors [17,18] and prisms [19,20], the bilens system can be used at high photon energies, up to 100 keV.

The problem of resolving the nanometer scale interference fringes in the near field is difficult because it requires special high resolution detectors. We circumvented this problem by inserting a 0.5 μm thick Ta grid with a 400 nm periodicity (200 nm slit and 200 nm bar) behind the bilens. We aligned the Ta grating parallel to the interference pattern generated by the bilens. The experimental setup for recording the interference pattern in the near field is depicted in Fig. 3(a). For this test we chose the second bilens with a focal distance of 35 mm at 12 keV. Intensity modulations are obtained by scanning the grid vertically across the fringes generated by the bilens. A *p-i-n* diode counting detector placed at 5 mm distance from the grid was used to record the intensity. To restrict the beam to the field of view of the grid, we used secondary slits 20 (V) by 20 (H) micrometers in front of the grid. The Ta grid was placed at a distance of 270 mm from the bilens, where the fringe periodicity is about 400 nm. The scan of the grid in the vertical direction is shown in Fig. 3(b). At the position of the grid along the optical axis when the pitches of the grid and interference pattern coincided, the contrast of intensity beating was maximal. Taking into account that the absorption of Ta grid at 12 keV is 6% and the interference contrast of the beam (38%), we can expect the visibility of fringes around 2.3%, which is very close to the measured one of 2%.

Another way of visualizing a nanopattern is to apply an imaging technique in which two periodical patterns with slightly different pitch sizes interfere to produce a moiré pattern. A moiré fringe pattern will be spaced at $\Lambda_m = p(1+\varepsilon)/\varepsilon \sim p/\varepsilon$, where p and $p(1+\varepsilon)$ are the grid and bilens fringe periodicity, respectively. Moving the 400 nm Ta grid along the bilens optical axis, we probed the pitch of interference pattern. The moiré fringes were recorded with an x-ray CCD camera located 5 mm from the Ta grid. The images recorded at different grid positions are shown in Figs. 3(c)–3(f). At the distance of 270 mm, the grid and the interference pattern pitch coincide, and moiré fringes are absent. Depending on the grid displacement from this position, the moiré pattern changes from 2 to 5 fringes with periodicity from 8 to 4 μm. We emphasize that the change in the number of fringes from 4 [Fig. 3(e)] to 5 [Fig. 3(f)] corresponds to a 5 nm increase of the bilens interference pitch size and a 3 mm longitudinal grid shift, demonstrating the extreme precision of the technique.

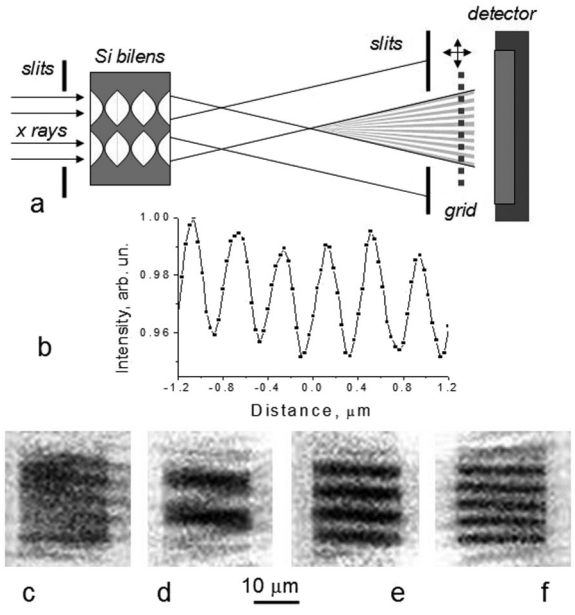

FIG. 3. (a) Layout for measurements of interference patterns in the near field. (b) Intensity modulations recorded with a *p-i-n* diode counter by scanning a Ta grid vertically. X-ray moiré patterns taken with a CCD camera for various distances between the bilens and the Ta grid: (c) 270, (d) 280, (e) 288, and (f) 291 mm.

In order to address the question of the smallest period of x-ray standing waves which can be generated by the bilens interferometer, let us consider the case of a fully coherent source as a point source at an infinitely long distance. In this case the incident wave can be treated as a plane wave. We restrict ourselves by the thin lens approximation. In this approximation, the compound lens composed of N double concave elements is equivalent to a single lens with an N times smaller radius of curvature. In the following we choose the lens length equal to $L = F/4$, the focal length as $F = R/2\delta$, and the lens geometrical aperture $A = 2(RL)^{1/2} = R(2\delta)^{-1/2}$. When the split distance d is equal to the lens geometrical aperture, the minimum distance where superposition of two beams starts is $z_1 = F$.

In this case, we obtain the minimum fringe spacing as $\Lambda = \lambda F/A = \lambda/(2\delta)^{1/2}$. As δ is proportional to λ^2, the fringe spacing is nearly independent of the x-ray energy and only twice larger than the smallest spot size to which x rays can be focused [21]. From this it would seen that high-Z materials are favorable; for example, for the gold bilens we calculate $\Lambda = 16$ nm. However, the absorption in high-Z materials drastically reduces the lens effective aperture. In the case of a gold bilens, the submicron aperture makes the use of such materials unfeasible. By taking the attenuation inside the lens into account, the minimum fringe separation can be achieved when the geometrical aperture and split distance are smaller than the lens effective aperture $A < A_{\mathrm{eff}}$, i.e., $R(2\delta)^{-1/2} < 0.47(\lambda R/\beta)^{1/2}$ or $R < 0.44\lambda\delta/\beta$. In this case, the radius of curvature strongly depends on the x-ray energy and lens material. The best performance is therefore expected for high density low-Z materials, such as diamond, silicon, and beryllium. So for silicon we have $\Lambda = 40$ nm, and an aperture $A > 20$ μm can be used above 50 keV. The best material would be diamond for which $\Lambda = 33$ nm, and $A > 20$ μm can be used for $E > 12$ keV. The beryllium bilens can generate fringes $\Lambda = 48$ nm in a broad energy range, and the largest aperture $A = 102$ μm is at $E = 20$ keV.

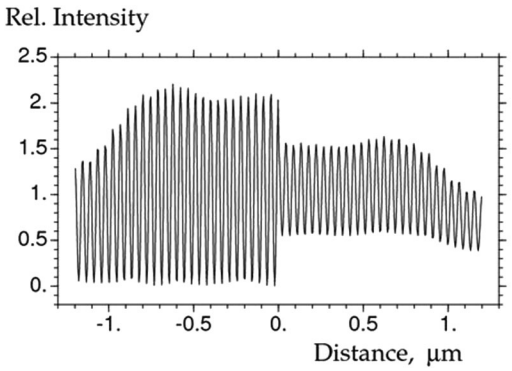

FIG. 4. Interference fringes for point (left) and 30 μm (right) source calculated for the parameters $E = 50$ keV, $A = 20$ μm, $d = A$, $R = 1.2$ μm, $N = 100$, $z_0 = 100$ m, and $z_d = 6.7$ cm.

The efficient use of the proposed bilens nanointerferometer depends not only on the resolution but also on the contrast of the interference field. As it follows from the fringe visibility formula (1), a 100% contrast corresponds to the distant point source. Considering a relatively transparent lens, we transform Eq. (2) as $S/z_0 < \alpha = 1.7(-\ln V)^{1/2}(\beta/\delta^{1/2})(1 - z_f/z_d)$. In the limit $z_f \ll z_d$ and for the 50% contrast, we obtain the upper limit for the angular source size $\alpha = 1.414(\beta/\delta^{1/2})$ depending only on the bilens material and x-ray energy. To verify the estimation made above, we performed computer calculations using the Kirchhoff propagator in a paraxial approximation. We find that the value of 0.25 μrad for the angular source size is appropriate for x-ray energies up to 100 keV. Figure 4 shows calculated interference fringes for a silicon bilens for point and 30 μm source.

In conclusion, we have demonstrated a new and simple way to generate an x-ray periodic interference field such as a standing wave with a variable period ranging from tens of nanometers to tens of micrometers. The proposed interferometer thus occupies the place between crystal [22] and grating interferometers [5–7]. Such coherent spatially harmonic illumination can be used for new diffraction and imaging methods to study mesoscopic materials. As we have shown, a coherent moiré imaging or radiography technique using a bilens is a straightforward application. The evident advantage of moiré radiography over the direct measurement of the interference fringes created by the bilens is that it greatly reduces the requirements on detector resolution while still offering a submicron and nanometer resolution. We would like to stress the fact that manufacturing of classical slits with nanometer opening sizes for high x-ray energies is a practical impossibility, as they would have to be extremely thick and resemble channels or waveguides. The bilens system has the advantage over double slits as it focuses x rays into the region where the two beams intersect, leading to an intensity gain factor for our nanointerferometer with respect to a hypothetical linear slit of 50 nm of at least 3 orders of magnitude.

As in the case of a classical interferometer, the bilens interferometer generates two coherent beams separated in space and then coherently recombines them to produce the interference pattern. One can easily insert a sample in one of the beams while they are separated. Any interaction with those beams will induce significant changes in the interference pattern, allowing the extraction of high resolution information on the sample from the new phase pattern produced. Contrary to Bonse-Hart interferometers and x-ray standing wave techniques, the bilens generates an interference pattern without the requirement of additional optics like crystals or multilayers. The interference occurs in air at a reasonable distance from the device itself, allowing great flexibility in sample size and environment.

Finally, the bilens interferometer can be used for coherence diagnostics at present synchrotrons. Si bilenses are stable under extremely powerful beams and relatively insensitive to mechanical vibrations.

[1] A. Snigirev *et al.*, Rev. Sci. Instrum. **66**, 5486 (1995).
[2] S. W. Wilkins *et al.*, Nature (London) **384**, 335 (1996).
[3] P. Cloetens *et al.*, J. Phys. D **29**, 133 (1996).
[4] C. Raven *et al.*, Appl. Phys. Lett. **69**, 1826 (1996).
[5] C. David, B. Nohammer, H. H. Solak, and E. Ziegler, Appl. Phys. Lett. **81**, 3287 (2002).
[6] F. Pfeiffer, C. Kottler, O. Bunk, and C. David, Phys. Rev. Lett. **98**, 108105 (2007).
[7] F. Pfeiffer *et al.*, Nature Mater. **7**, 134 (2008).
[8] W. Leitenberger, S. M. Kuznetsov, and A. Snigirev, Opt. Commun. **191**, 91 (2001).
[9] W. Leitenberger, H. Wendrock, L. Bischoff, and T. Weitkamp, J. Synchrotron Radiat. **11**, 190 (2004).
[10] D. Paterson *et al.*, Opt. Commun. **195**, 79 (2001).
[11] A. Snigirev, V. Kohn, I. Snigireva, and B. Lengeler, Nature (London) **384**, 49 (1996).
[12] V. Aristov *et al.*, Appl. Phys. Lett. **77**, 4058 (2000).
[13] C. G. Schroer *et al.*, Appl. Phys. Lett. **87**, 124103 (2005).
[14] A. Snigirev *et al.*, Proc. SPIE Int. Soc. Opt. Eng. **6705**, 670506 (2007).
[15] M. Born and E. Wolf, *Principles of Optics* (Cambridge University Press, Cambridge, England, 1999).
[16] V. Kohn, I. Snigireva, and A. Snigirev, Phys. Rev. Lett. **85**, 2745 (2000).
[17] K. Fezzaa *et al.*, J. X-Ray Sci. Technol. **7**, 12 (1997).
[18] W. Leitenberger and U. Pietsch, J. Synchrotron Radiat. **14**, 196 (2007).
[19] A. R. Lang and A. P. Makepeace, J. Synchrotron Radiat. **6**, 59 (1999).
[20] Y. Suzuki, Rev. Sci. Instrum. **75**, 1026 (2004).
[21] C. Bergemann, H. Keymeulen, and J. F. van der Veen, Phys. Rev. Lett. **91**, 204801 (2003).
[22] U. Bonse and M. Hart, Appl. Phys. Lett. **6**, 155 (1965).